Dynamic aberrometer/topographer designed for clinical measurement and treatment of highly aberrated eyes

Daniel R. Neal,* Xifeng Xiao, Richard James Copland, Lyle Kordonowy, Dan Hamrick, Daniel Medina, John Dixson, Phil Riera, Paul Pulaski, Tristan Turner, Jeff Kolberg, Ron Rammage, Steve Farrer, Dean Rusk, and Matt Haugo

WaveFront Dynamics Inc., Albuquerque, New Mexico, United States

Abstract. The human eye is a complex optical system with multiple elements. It is aspheric, nonsymmetric, and time dependent; yet, overall it has incredible performance. There have been various instruments developed over the years to measure and then to guide treatment to correct for ocular aberrations. As the development of these instruments (and treatments) has progressed, we have sought to correct more difficult cases, which may be more aberrated, time-dependent, or difficult in some other way. To this end, we have developed a new dynamic aberrometer that expands the boundaries of measurement capability with the aim of measuring and treating more difficult cases. This aberrometer has been designed that incorporates high-resolution Shack–Hartmann wavefront sensing, full gradient (spot) corneal topography, dynamic acquisition, and a subjective digital refractometer. This instrument is designed to measure extremely high aberrations and to provide information for treatment in multiple modalities. A small clinical study was conducted with subjects ranging from 23 to 64 years old to evaluate the effectiveness of the dynamic analysis at selecting a refraction. Examples are presented for measurements with keratoconus, irregular corneas, and tear-film irregularity. In the clinical study, young subjects showed an overall +0.27 D reduction in instrument induced myopia using dynamic measurement compared to a snapshot. The instrument has a large dynamic range for measuring subjects with keratoconus and other aberrated corneal conditions. The new instrument is effective at providing information needed for treatment in multiple modalities. The subjective digital refractometer corrects the fixation target for the objectively measured low-order aberrations (defocus and astigmatism). This provides immediate subjective feedback on the objective refraction and, with the ability to manually adjust the refraction parameters, the ability to compare objective and subjective refractions in the same setting. [DOI: 10.1117/1.OE.61.12.121808]

Keywords: wavefront; aberrometer; topographer; tear film; phoropter; digital refractometer.

Paper 20220582SS received Jun. 1, 2022; accepted for publication Nov. 9, 2022; published online Nov. 30, 2022.

1 Introduction

More than 400 years ago, Scheiner realized that optical aberrations influence image quality. He even made attempts to measure the aberration of the human eye through off-axis small-aperture measurements (the Scheiner disk).[1] Over the years, there have been many different aberrometers developed,[2] including both subjective and objective variants.[3,4] Williams and Liang[5] developed a complete adaptive optics system that could not only measure the aberrations but could correct them for visual experiments or retinal imaging. The advent of laser refractive surgery (LRS) led to several innovative ways to measure the aberrations of the eye since the process both induced aberrations and had the potential to correct them. Various technologies were developed including Shack–Hartmann (or Hartmann–Shack) wavefront sensor (WFS),[6]

*Address all correspondence to Daniel R. Neal, dan.neal@wavdyn.com

Tscherning aberrometer, dynamic sciascopy, injection raytracing, and pyramid wavefront sensing. These all have unique advantages and disadvantages. However, many of these approaches are limited in the aberration measurement magnitude or accuracy. Several generations of instruments have been developed for wavefront guided (WFG) LASIK or PRK.

WFG LRS has challenged the measurement capability of aberrometers ever since it was first attempted. The idea seems simple: to measure the aberrations and to modify the ablation map to correct them. However, in practice, this is far from simple. The measurements must be accurate and repeatable, and they must have sufficient dynamic range to cover the magnitude of the aberrations present. The treatment is on the cornea, but the wavefront aberrations are measured through the pupil. The shape of the cornea affects the laser ablation efficacy. In addition, the laser itself may induce some aberrations and the cornea may respond to the surgical process through biomechanics or epithelial remodeling. Nevertheless, outstanding results have been obtained using this method, and it is now the standard of care in many practices.[7]

LRS is limited to ablation of the cornea and, as such, it must have sufficient corneal material to work with. With the advent of thin-flap femtosecond laser flap-makers, there is sufficient cornea remaining for most treatments over quite a large refractive range, except for thin corneas. A thin cornea, or a cornea with a weak spot (i.e., keratoconus), has a greater risk of ectasia and hence is generally avoided in most LRS practices. In fact, in most clinics, considerable effort is expended to identify and screen out those with form-fruste keratoconus or other corneal abnormality. Unfortunately, it is these people who are likely to have the greatest need for a WFG treatment.

Keratoconus has an incidence of about 1 in 2000 (CLEK study,[8] others). However, with the development of better metrology equipment, this is more recently estimated at 1 in 375, or nearly 0.5% of the population.[9] Generally, these people are not eligible for LRS and have few options available to them for high-quality vision.

There continues to be improved methods for treatment. Scleral contact lenses have been developed to provide a regular surface that is not dependent on corneal shape. These lenses rest on the sclera and vault so that they do not touch the cornea. As the space between the lens is filled with tear film, any irregularities in the anterior cornea are corrected. This provides relief for many patients.

Unfortunately, keratoconus (and pellucid marginal degeneration, scars, etc.) affect the posterior cornea as well. Thus the aberrations are not fully corrected by a scleral contact lens designed to neutralize the imperfections of the anterior corneal surface. In many cases, the scleral contact lens corrects about 20% to 50% of the aberrations but inverts the aberration map (see Fig. 1). This can still leave significant uncorrected aberrations in the eye's optical system. This is a good opportunity for attempting a WFG correction.[10,11] Wavefront correction can be applied to contact lenses, phakic and pseudophakic IOLs, and perhaps even to the cornea itself. Multiple approaches to wavefront correction of the whole eye aberration have been demonstrated by various researchers over the years.[10,11]

However, these patients are among the most aberrated, and we need an instrument that has the right combination of features for making accurate measurements of highly aberrated eyes. It also should be able to evaluate the position, rotation, and stability of various types of contact lenses, and preferably provides information for screening and fitting as well. This places some challenging requirements on the instrument, including multimodality, wide eye image field of view, high dynamic range, and dynamic acquisition; and of course, it must be accurate and repeatable.

2 Instrument Design

2.1 *Measurement Limitations*

2.1.1 *Resolution, dynamic range, and accuracy*

An important consideration in any instrument design is the resolution and dynamic range of the measurement system. For a Shack–Hartmann system, previous work has established the

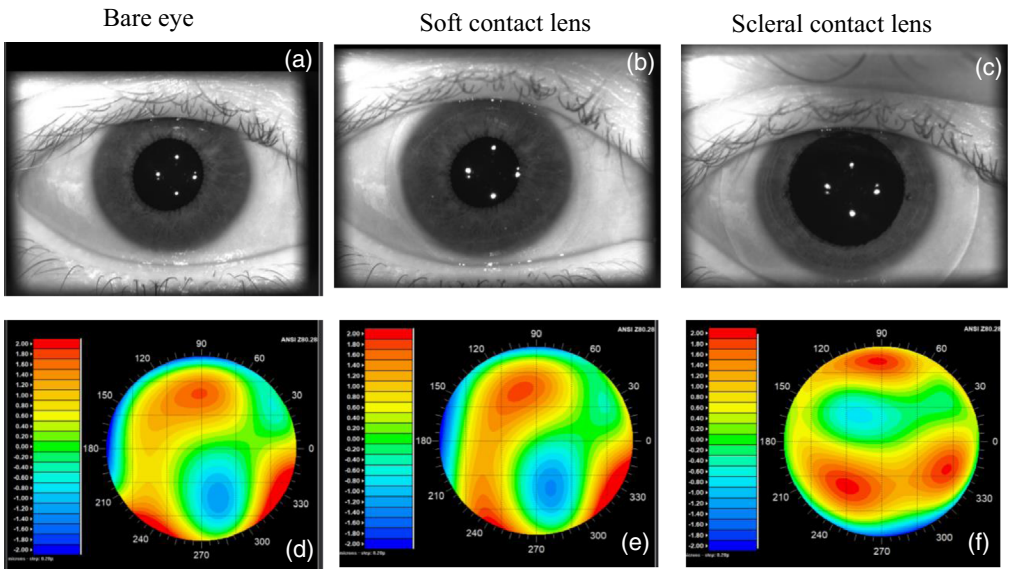

Fig. 1 Wavefront measurements of a keratoconic eye with 5.5-mm analysis pupil diameter for (a), (d) bare eye, (b), (e) corrected with soft contact lens, and (c), (f) corrected with scleral lens. (a)–(c) Their respective Scotopic iris raw images and (d)–(f) their respective HOA map.

advantages of higher resolution systems.[12] The lenslet Fresnel number is often the limiting factor in dynamic range and accuracy.[13,14] However, the aberrations of the eye are generally smoothly varying. Although the tear film can change on smaller scales,[15–18] the actual wavefront amplitude changes are quite small over the sample area and so smaller samples are more likely to be piecewise planar over the lenslet array.[13–15] This means that for regions of the wavefront with large wavefront variations the spots move together in groups, expanding and contracting the spot spacing. Thus it is possible to exceed the strict limits on dynamic range imposed by previous design approaches if a software algorithm is used to track the spots over these regions.[14] Several such approaches are now practical with advances in computer technology.[19]

As the aberrations and even refraction of human eyes are not precisely known and the eye itself is constantly changing, it is difficult to discuss accuracy of the instrument in the direct context of ocular measurements. Repeatability can certainly be determined, but even that may be due to variability in the eye itself, rather than to some feature of the instrument. Generally, we use test objects to determine instrument accuracy and precision of the measurement process. However, measuring a test object is not the same as measuring the eye, which has enormous variability, is constantly in motion, and may have errors induced by the measurement process itself. Ultimately, it may be the efficacy of a correction derived from the measurement that is a measure of the overall accuracy of the instrument in measuring eyes.

The accuracy of the sensor is determined partly by the number of pixels[13] involved in the centroiding algorithm and partly by the number of spots.[12] In Table 1, we show the parameters for the instrument described herein. Previous instruments designed by the same team have been included for reference. On test optics, typical root-mean-square (RMS) noise level is $<0.02\ \mu$m (full aperture). The system calibration is usually limited by the accuracy of calibration optics but is usually better than 0.008 D over the full range.

Although there is a trade-off between the number of lenslets and the pixels per lenslet,[14] with the extended dynamic range (EDR) algorithm, high-resolution sensor and high speed, 2048×1536 pixel camera ($\sim 21 \times 21$ pixels per lenslet), it is possible to greatly extend the range of measurable eyes.[17] Thus the dynamic range exceeds $+12$ to -25 D in sphere and 14 D in cylinder. Figure 2 shows an example where the internal wavefront measurement had significant residual error. This caused the focal spots to move out from behind their associated lenslets, which would be beyond the dynamic range using traditional methods. Figures 2(a) and 2(b) shows how this affects the data analysis, adding significant noise and error. In Figs. 2(c) and 2(d), the EDR algorithm was used to progressively analyze the data in annular regions, starting

Table 1 Instrument specifications comparison to previous instruments.

Instrument	Unit	COAS-HD	iDesign	WaveDyn
Specifications				
Input aperture *X*	mm	12.2	10.8	11.5
Input aperture *Y*	mm	8.6	8.6	8.6
Dynamic range of 7 mm pupil	D	3.6	3.9	7.3
Samples in 7 mm pupil		1427	1226	2821
Spatial resolution	mm	0.164	0.177	0.117
Noise floor (RMS WFE)	um	0.031	0.010	0.005
Pixels/lenslet		16	21	21
Pixels/focal spot		33	46	62
WF lenslets *X*		74	61	98
WF lenslets *Y*		53	49	74
Max power (7 mm)	D	3.6	3.4	8.3
Max cylinder	D	7	6.8	16.7
Min sphere (full aperture) IR	D	−12	−16	−12
Max sphere (full aperture) IR	D	6	8	12
Min sphere range (7 mm)	D	−15.6	−19.4	−25
Max sphere range (7 mm)	D	9.6	11.4	12
Iris image FOV *x*	mm	18	18	24
Iris image FOV *y*	mm	13	13	18

with the central 1.5 mm region. Search areas were identified by extrapolating polynomial fits to identify the next set of focal spots. Then the region was expanded iteratively. In Figs. 2(c) and 2(d), the resulting wavefront shows a smooth transition with no evidence of out-of-range conditions. Note that refraction magnitude is reduced and that the RMS wavefront error is much less in magnitude as the out-of-range errors were mitigated.

2.1.2 *Instrument induced accommodation by the eye*

One key limitation of many autorefractors and aberrometers is the interaction between the patient and the instrument.[20,21] Placing a large instrument in close proximity to the patient's eye will often induce accommodation, thereby giving an inaccurate measurement. There are several other factors that can also lead to instrument induced accommodation.

- *Single snapshot measurement*. The eye, especially for younger subjects, is constantly moving and adjusting. Therefore, it is difficult to identify a single measurement snapshot that is representative of these constantly changing imaging conditions.
- *Poor fixation target image*. If the target is not clear enough to the subject, it will provide little guidance for proper fixation. This may be worse if the subject has significant aberrations.
- *Inadequate fixation target compensation for focus and astigmatism*. The presence of uncorrected cylinder leads to different apparent image planes. This creates confusion since lines at different angles will effectively focus at different planes.

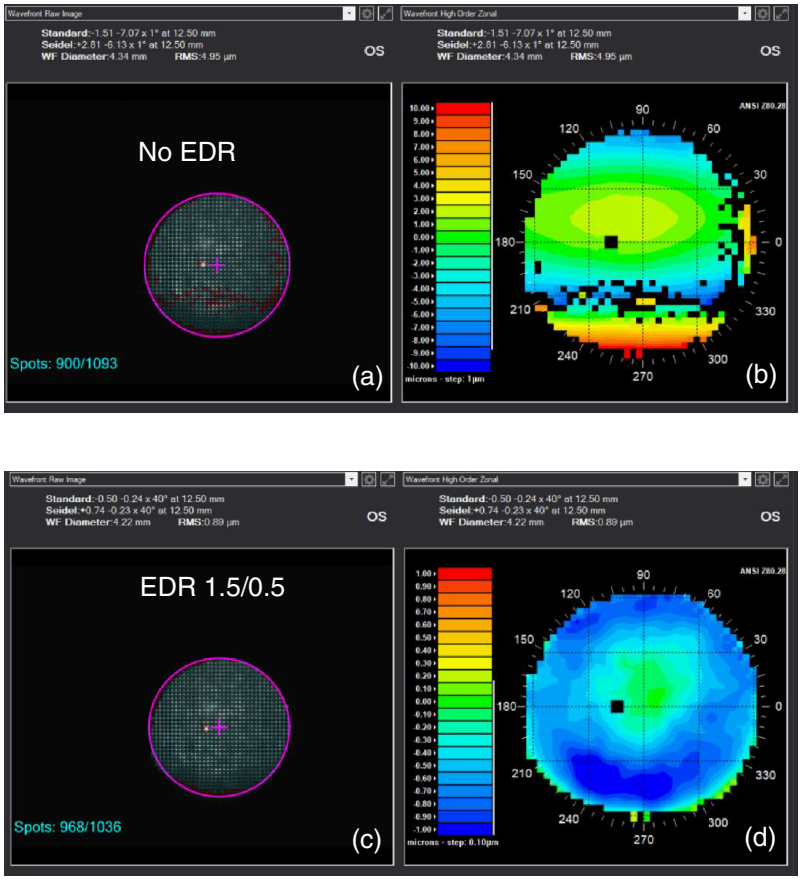

Fig. 2 Example wavefront that exceeds the dynamic range limits of classical Shack–Hartmann WFS system. (a) Raw image from the Shack–Hartmann sensor with an overlay showing good spots and (b) zonal reconstruction derived from the measured spot positions, when no EDR is applied. Note in (a) noise in bottom third where spots exceed the dynamic range. (c), (d) The same counterparts as (a) and (b) when EDR is applied. The EDR analysis is implemented where the data were progressively fit in annular regions starting with 1.5-mm radius in 0.5-mm steps. Note that the algorithm successfully tracks the focal spots across the entire pupil.

- *Insufficient or inappropriate fogging*. Fogging is used to encourage the patient to focus at the far-point or distance refraction. If there is insufficient fogging, then the patient may not try to focus or only focus within the accommodative lag. If there is too much fogging, then the subject only sees a blur, which gives no clues for accommodative response.[22,23]
- *Presence of high-order aberrations leads to uncertainty of subjective refraction*. Since the refraction parameters (sphere/cylinder/axis) do not affect the higher orders, a subject with significant higher order aberrations (HOA) may have a large range where there is little difference in the apparent image quality. For these subjects, the subjective refraction is often significantly different from the objective refraction and may also be imprecise.

The next section describes the instrument's basic design and important features.

2.2 *Requirements*

The key requirements can be identified by considering the desired applications. The conceived instrument would incorporate a Shack–Hartmann WFS, corneal topographer, eye imaging system, patient fixation system, and patient alignment stage, and of course it will need a computer, chinrest, and optomechanical structure. The instrument is intended to be a stand-alone

instrument. As space in most clinics is limited, it is desirable that the instrument size be as small as possible and that it be able to replace one or more existing clinical instruments.

2.3 *Optical System*

The optical system consists of multiple, co-aligned optical paths as shown in Fig. 3. These include the eye-image, light injection, WFS, patient fixation, corneal topographer, and rangefinder. These various paths are aligned relative to each other with very tight tolerances (<0.1 mr).[24] This is possible using the built-in WFS as a reference, as the WFS provides extremely precise alignment information. A fiber-coupled super luminescent diode (SLD) is used as a source for the WFS since this provides a point source of light with low temporal coherence (to minimize speckle).

2.4 *Eye Imaging System*

One key goal of this instrument is the ability to measure position and stability of contact lenses on the eye while simultaneously measuring the wavefront aberrations. Scleral lenses are in common use that have diameters of 18 to 19 mm. Thus the field of view of the eye-image

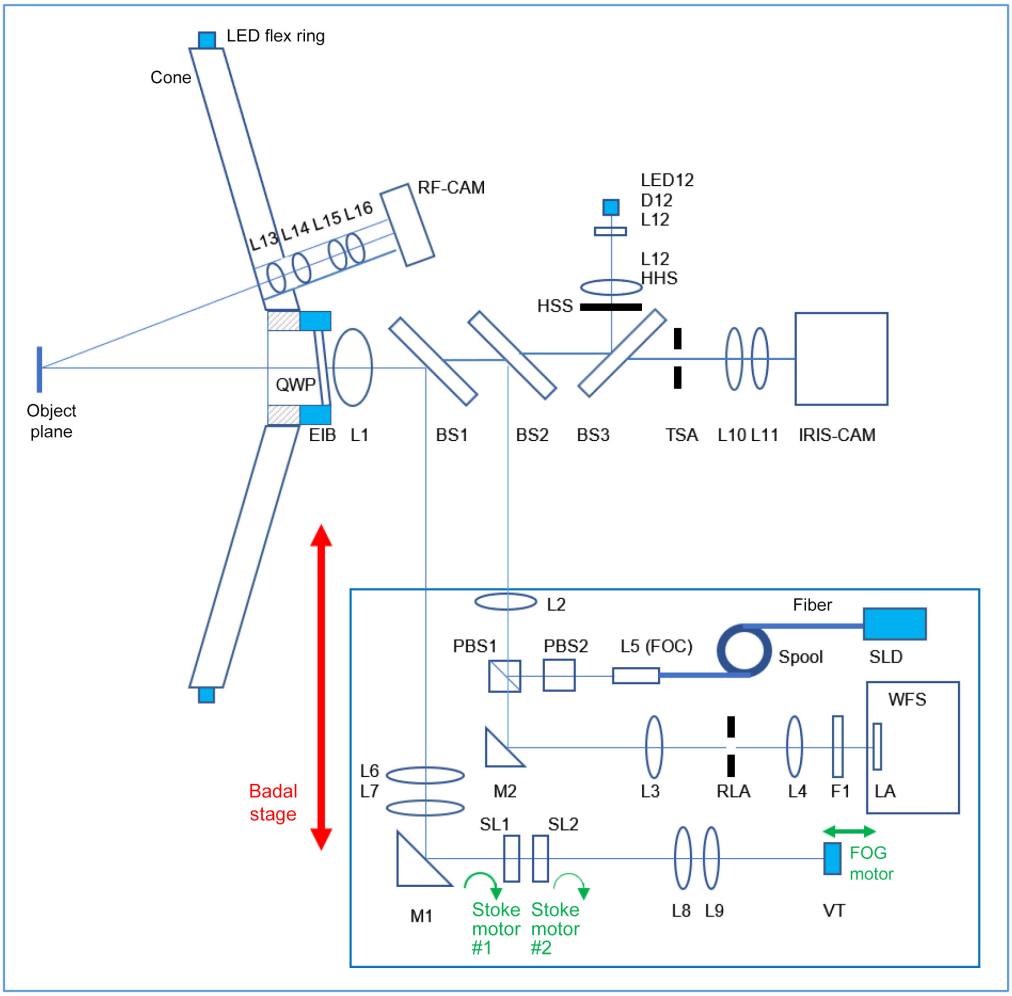

Fig. 3 Schematic of the aberrometer optical layout. Note: L, lens; M, mirror; QWP, quarter wave plate; BS, beam splitter; PBS, polarized BS; CAM, camera; TSA, telecentric stop aperture; RF, range finder system; SL, Stokes cell lens; VT, video target; FOG, fogging motor; and HHS, Helmholtz source.

subsystem must be at least 20 mm. It is also desirable to use a telecentric optical system to avoid changes of magnification with defocus, so this requires a quite large main objective. For the new instrument, a 30-mm custom lens was designed, with a 24×18 mm FOV. The system was also designed with a 6-mm depth of field so the cornea and iris can be imaged simultaneously. This allows imaging small marks (fiducials) on the contact lens while still imaging the pupil. The high-resolution image can also be used to measure the pupil and iris boundaries.

2.5 *Aberrometer*

The aberrometer consists of a Badal imaging system to adjust the focus to match the spherical equivalent of the eye. The SLD is prefocused by this same system so that it creates a small focal spot on the retina. The light scattered from the retina is imaged onto a Shack–Hartmann WFS, which is used to control the Badal defocus in a simple control loop.

The WFS is a custom micro-optic, made with photolithography and plasma etching. This process provides an extremely accurate lenslet with very small features. The plasma etching process results in no dead space between lenslets, which minimizes any sources of noise or crosstalk. The resulting sensor has 98×74 samples with more than 7200 measurement points across the sensor. With an appropriate magnification to match the sensor size to typical maximum pupil size, this provides >2800 points across a 7-mm pupil. In addition, the pixel density $\sim 21 \times 21$ pixels/spot provides reasonably good resolution for every point spread function, which can provide more details than just the centroid and hence may be important in light scatter and microaberrations produced by tear film breakup and/or cataracts.

One of the key goals of this new instrument is the ability to measure much more aberrated eyes. The large objective lens facilitates light collection for rays with significant deviation. The lenslets were designed with a modest Fresnel number (~ 4) to facilitate good spot detection accuracy. Normally this would lead to a reduction in the available dynamic range. However, since the samples are so small on the eye (0.116 mm), software is used to track the spots as they move in groups. Although there is still an internal aperture to reduce background light, this is relatively large to allow for measurement of extremely aberrated eyes.

2.6 *Topographer*

The topographer resembles a Placido disk system, with a cone that is similar in size to many other topographers. However, instead of rings, a full-gradient topography (or spot-based) system is used. The spots provide a direct measurement of the surface slope in two orthogonal directions, facilitating more direct interpretation of the surfaces. With the large objective lens, there is a large amount of data that is potentially lost right in the center of the optical system. This missing data are filled in by projecting light through a mask to provide a grid of spots on axis. Thus there is no region of the cornea that is unsampled.

2.7 *Rangefinder*

With a telecentric optical system that has a large depth of focus, it is more difficult to use imaging of the iris as a means for setting the appropriate distance between the instrument and the eye. A means for accurately measuring the true distance is needed. To this end, a separate "rangefinder" camera was used to view the eye at an angle. The eye-instrument distance can be computed using triangulation.

2.8 *Dynamic Acquisition System*

All the cameras and light sources were controlled with custom electronics boards that provide synchronization between the various light sources and cameras. This provides software control of the various acquisition modes, which allows for flexibility to implement various workflows. The system is capable of up to 120 fps for single-channel acquisition, with typically 54 fps in multiplexed cases (wavefront and image or wavefront and topography).

2.9 *Integrated Subjective Digital Refractometer*

To obtain accurate measurements of the refractive state of the eye, it is important to include an appropriate fixation target and associated optics.[20] Previous instruments (COAS, iDesign) have incorporated the fixation target on the Badal stage to provide appropriate adjustment and fogging but have not compensated the target for astigmatism. For these instruments, it was found that instrument accommodation was prevalent in subjects with high astigmatism. Thus for the new instrument, an astigmatic correction system was developed. This consisted of a Stokes' cell, which is a pair of cylinder lenses of opposite powers, mounted in cells that can be rotated relative to each other. Combined with an additional motor on the fixation target itself, the fixation target can be controlled for combinations of sphere, cylinder, and axis. Since the target itself is a pixelated programmable display, this essentially incorporates all the features of a subjective digital refractometer.

The subjective refractometer is initialized from the measured wavefront during the autorefract sequence, and the final measurement is presented to the patient as a verification that the refraction measurement provides the best correction. Since the WFS and the fixation channels are separate optical paths with independent calibrations, this verification is an immediate check on the overall quality of any given measurement. The user is provided with manual controls so that he/she can adjust the parameters (sphere, cylinder, or axis) to provide subjective confirmation.

The fixation target is an 800×600 programmable display with 1.6 arc min /pixel resolution. This can be programmed with letter charts, images, moving images (GIFs), and geometrical targets. The targets can be either static or dynamically presented with user control of the timing and synchronization. The user can also select the brightness as desired. This size target will provide up to ± 8 deg angular field.

This provides the user with a basic digital phoropter, built into the instrument. The fixation path can be corrected with ± 3 D of additional sphere (on top of the ± 12 D Badal system) and up to 6 D of cylinder in 1-deg increments. These can be controlled either automatically or manually by the user. This, in conjunction with the video fixation target, provides for many options in evaluating subjective response in parallel with the objective measurement. Since the target is also viewed through the Badal system, the instrument can be programmed to provide varying apparent axial positions in timed steps. This provides a mechanism for the potential measurement of accommodative range and for psychophysical research. This same sequence can also be programmed by the user to present a sequence of off-axis fixation targets to quickly measure the refraction and aberrations along multiple axes.

2.10 *System*

The resulting system specifications are presented in Table 1. The schematic of the system optical layout is presented in Fig. 3 and a photograph of a prototype instrument is shown in Fig. 4. The software has a modular architecture to facilitate the various workflows and parallel processes. The instrument is designed to be operated dynamically with sequences that may last 10 to 30 s. To avoid undue delay in data analysis, the analysis operates in parallel with the acquisition in a separate thread. Thus all the analysis is completed shortly after the acquisition is finished. The data acquisition, data analysis, and data viewer are modular programs that work together to support the different functions. Depending on users' desire and/or preferences, the data acquisition graphical user interface (GUI) supports customized acquisition with different workflows, controls sequence timing, digital refractometer, and hardware functions (Fig. 5). Due to its wide degree of flexibility, the instrument can serve several different purposes, from clinical measurement and treatment to research. The data viewer provides maps and control of data review for all the various wavefront, refraction, and topography maps (Fig. 6) and can be installed on an external computer as needed. Data can be exported for each image, analyzed frame, and sequence summary in tagged format. Wavefront data can be analyzed to produce all-order and high-order modal (Zernike) and zonal maps, irregularity, raw image, polynomial coefficients, point-spread-function, and simulated images. Corneal topography (CT) analysis includes axial power, mean curvature, refractive power, tangential curvature, sphere elevation, ellipsoid

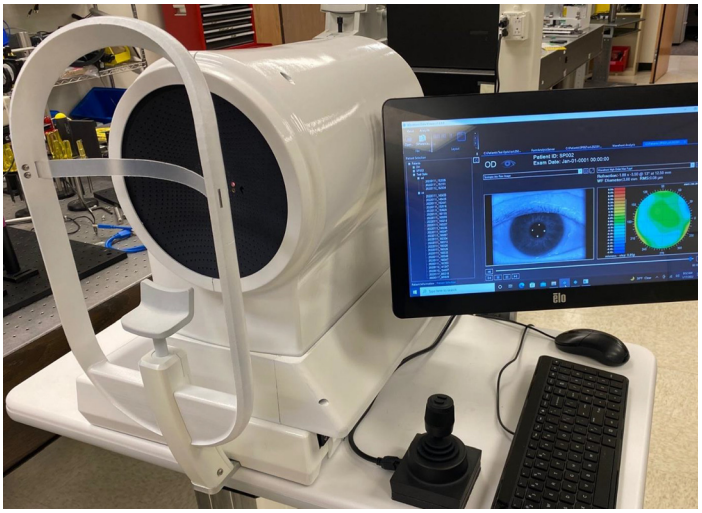

Fig. 4 Photograph of prototype instrument. The adjustable monitor arm provides operation in many different settings and gives the operator options for working with the patient during the measurement process.

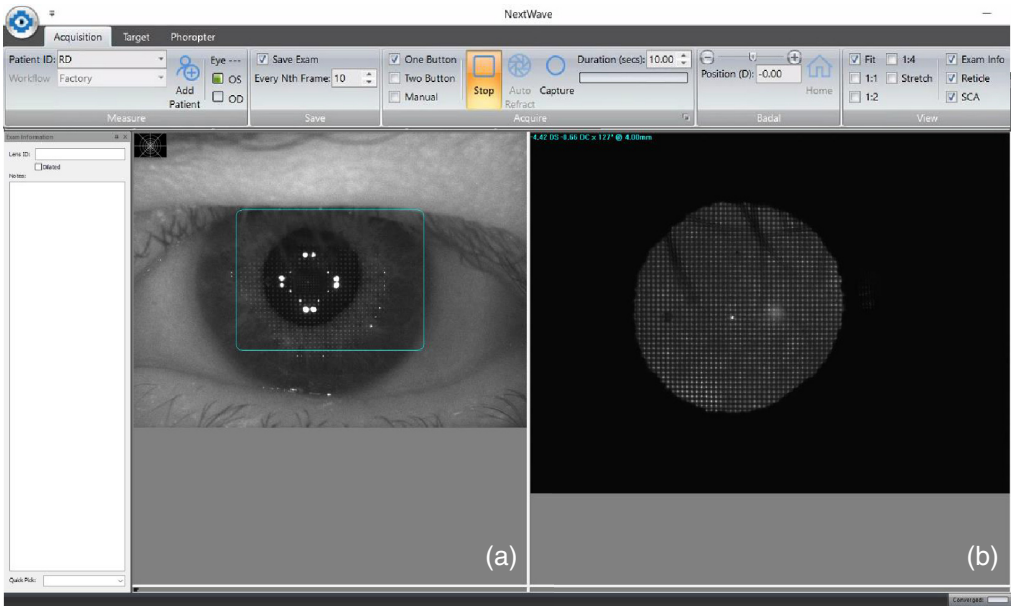

Fig. 5 Data acquisition GUI with (a) live iris (with CT illumination) and (b) raw wavefront and refraction. The highlight rectangular area is WFS camera's field of view in iris camera.

elevation, population ellipsoid elevation, irregularity, corneal aberrations (all and high order), raw image, and eye images.

3 Objective and Subjective Refraction

Since the eye is a dynamic optical system, changing within each blink, it is subjectively difficult to observe the variations quantitatively. During a typical visual task (determining visual acuity on an eye chart for example), a single number may be determined through patient feedback. However, this represents the best measurement that was obtained by the optical system during the time allotted. This is one reason it is difficult to compare the objective and subjective measures.[25–28] Nevertheless, these comparisons are necessary, as a refractive correction is almost

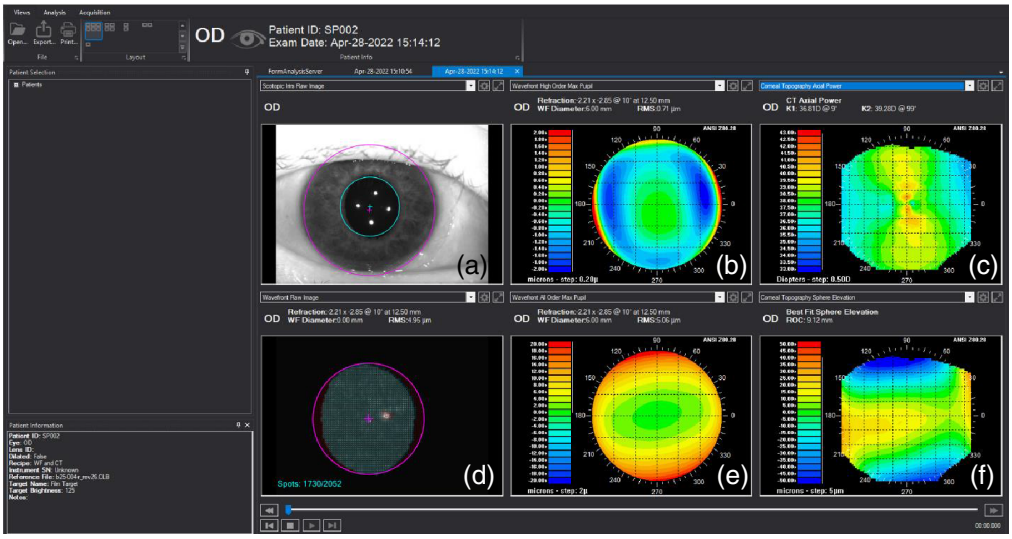

Fig. 6 Data review screen with (a) eye image, refraction, (b) higher order analysis, (c) CT axis power, (d) WFS raw image, (e) all order analysis, and (f) best fit sphere elevation.

always a single fixed optic. Even for a WFG correction, only one set of HOA optics may be built into the correcting lens. So it is important to be able to analyze the sequences and determine a "selected" examination that represents the intended best correction.

Figure 7 shows the dynamics of the refraction terms (sphere and cylinder) for a 23-year-old female subject. It is evident that these values vary in time during the measurement sequence. The wavefront and iris images were recorded at the maximum rate. This resulted in 54 frames/sec acquisition rate or 541 frames of data in a 10-s sequence. Note that the sphere varies by as much as 0.3 D during this sequence with some (although less) cylinder variation. Blinks were removed to minimize outliers in the data.

There are several methods that may be used to identify the parameters that would lead to a best correction.

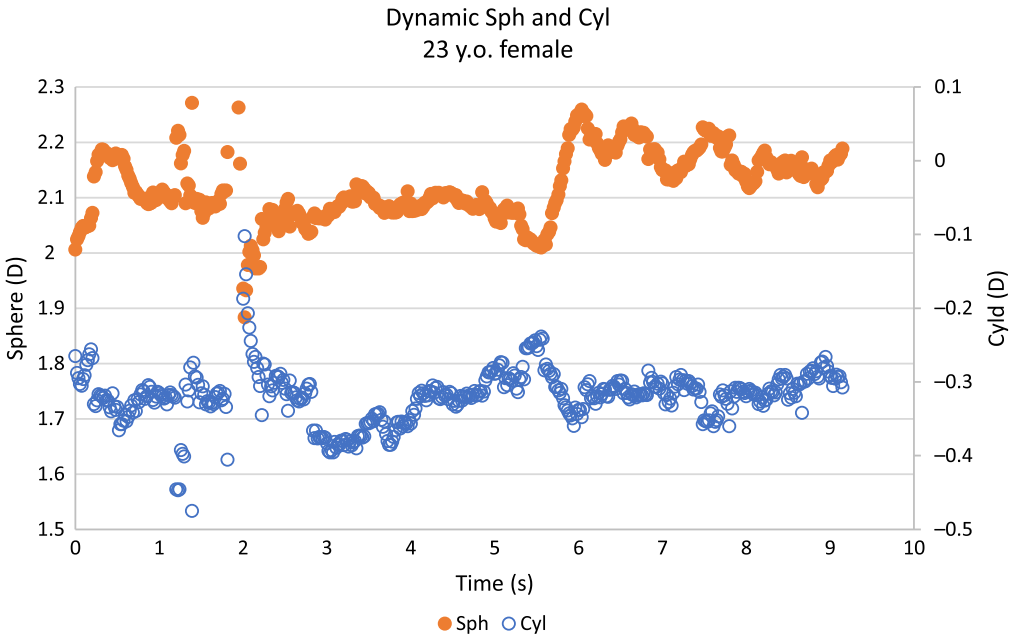

Fig. 7 Dynamic analysis of sphere and cylinder for a 23-year-old female subject over a 10-s period. Data recorded at 54 fps.

- *Blink removal and detection.* Blinks must be identified and removed from any averaging or optimization operations. In addition, blink identification can aid in interpretation of tear film or other dynamic effects. Blinks can be identified by looking for changes in pupil size, wavefront diameter, light return or through a more sophisticated image processing algorithm. As the natural blink can happen quickly, at low-acquisition rate they can be difficult to detect.
- *Averaging.* After removing blinks and outlier measurements, averaging the parameters over the time sequence may be appropriate. This is particularly true of HOA that are relatively unaffected by accommodation. In fact, it may be desirable to average variations caused by tear film or other transient phenomena.
- *Optimization.* For some parameters (in particular, the spherical equivalent) that are affected by subject accommodation, the "selected" result may be determined through some combination of the magnitude, the pupil size, and the measurement data quality (and/or other parameters). To this end, we have introduced a merit function (MF) that weights the various parameters and then optimized this MF over the sequence. This results in selected exam that may be used for treatment or evaluation. The MF is defined as follows: first, a normalized parameter function is defined as

$$\hat{P}(k) = \frac{P_k - P_{\min}}{P_{\max} - P_{\min}}, \tag{1}$$

where $\hat{P}$ varies from 0 to 1 (min to max) within the sequence P_k. P_k can be any measured parameter such as pupil diameter (D), spherical equivalent (S), image quality (I), or some other parameter. The MF is then constructed by weighting the various normalized parameters:

$$\mathrm{MF} = \frac{W_S\hat{S} + W_D\hat{D} + W_I\hat{I}}{W_S + W_D + W_I}, \tag{2}$$

where W_x ($x = S$, D, or I) represents the weighting values. This MF can be searched for the maximum value in the sequence to find the selected exam k. It may also be advantageous to filter the parameters with running averages to minimize noise and outliers.

4 Results

4.1 *Example Measurements*

A rigorous verification and validation process was conducted on the first instruments before releasing for human eye measurement. Multiple model eyes with the known and exact diopters and diameters were measured and favorably compared with their specifications. Less than 1% of differences were obtained in each measurement.

Figure 8 shows a wavefront measurement for a 42-year-old male subject with moderate keratoconus. For a fixed analysis pupil of 5.50 mm, his wavefront aberrations were 0.63 μm RMS, which is above the normal range. In (a), the HOA wavefront measurement for his bare eye is presented, and (b) is the HOA with a scleral lens. His vision was corrected with a scleral lens to reduce his aberrations. However, while the scleral lens reduces his low-order refraction, it did not change the higher orders in this case. In fact, the higher orders are nearly the same magnitude but inverted in sign.

The tear film can be evaluated from both the wavefront and the topography by plotting the residual after subtracting fit polynomials. In Fig. 9, the Zernike polynomials through sixth order were subtracted from the zonal wavefront map. This shows irregularities in the wavefront, which are a good indication of tear film irregularity.[29] The irregularity grows in strength until the blink as shown in each successive frames (a)–(f) with time from 0 to 1.435 s with 0.285-s interval. Changes in the irregularity are often the result of tear film variations.

The spot-based topographer is designed to be able to measure the shape of unusual eyes without assumptions. As each spot provides information about the surface gradient in both

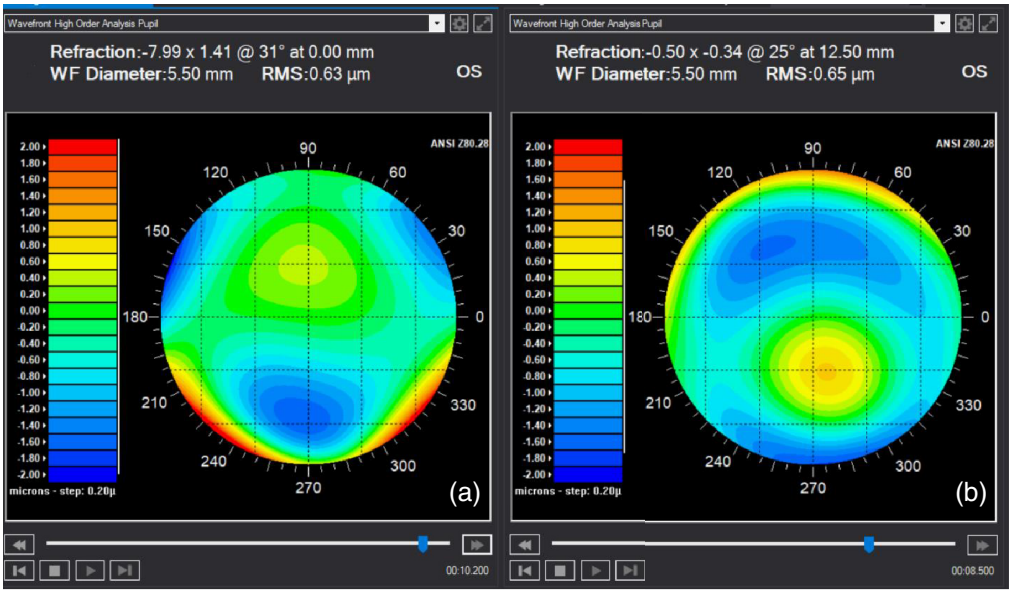

Fig. 8 Higher order wavefront map for a 42-year-old. male patient with moderate keratoconus. (a) Bare eye (no correction) and (b) correction with a scleral lens.

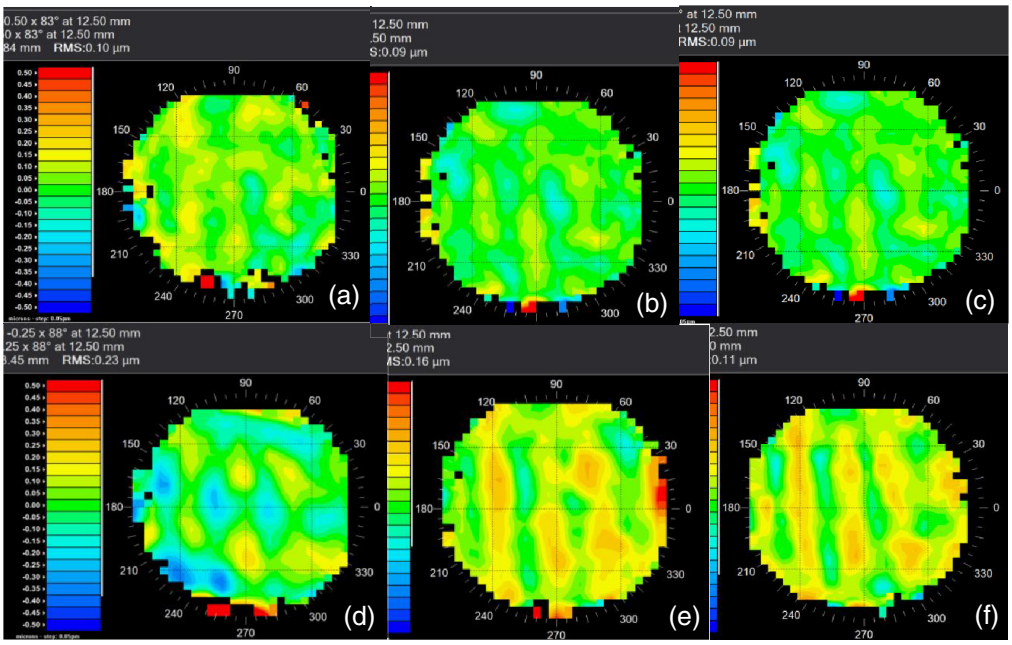

Fig. 9 Example tear film measurement from time (a) $T = 0.0$ s, (b) 0.29 s, (c) 0.57 s, (d) 0.86 s, (e) 1.15 s, and (f) 1.44 s.

x and y directions, the surface reconstruction does not rely on any assumptions other than that the surface is continuous. Thus this provides good information for highly irregular corneas. An example of a keratoconus CT measurement is shown in Fig. 10. The maps have an irregular outline because of the shadows caused the by subject's nose and eyebrows. It is possible to reduce these shadows by tilting the subjects head slightly temporally. However, since these measurements are made simultaneously with the wavefront measurements, often it is desirable to measure both wavefront and topography in the same orientation as normal patient fixation, that is, straight ahead.

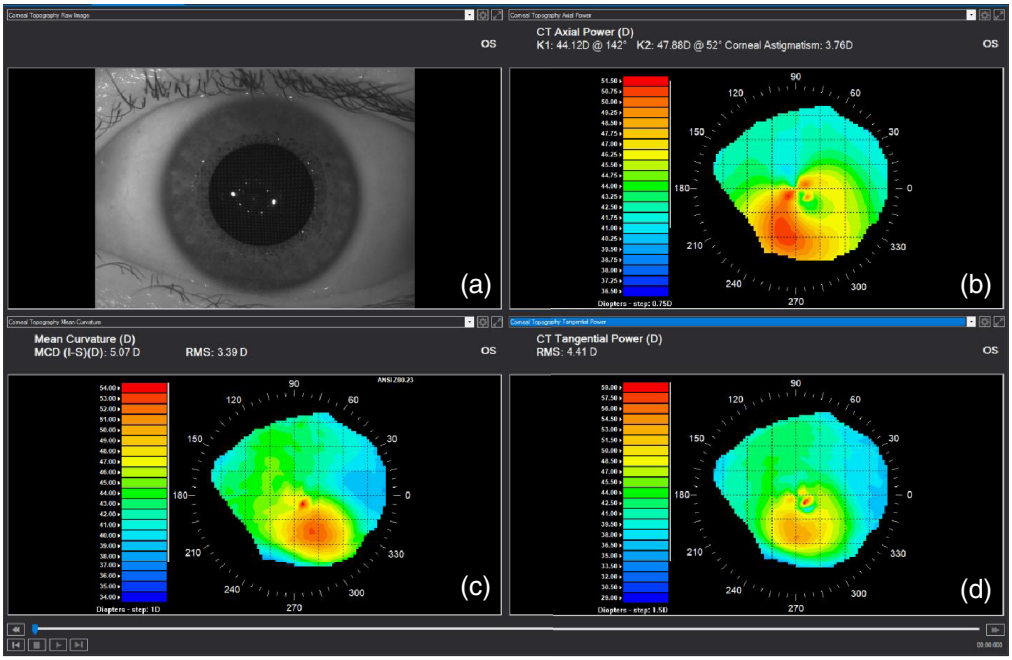

Fig. 10 CT results from a keratoconus subject: (a) eye image with CT illumination, (b) CT axis power, (c) mean curvature, and (d) CT tangential power. The irregular shape of maps from (b) to (d) is the result of shadows from subject's nose and eyebrows.

Figure 11 shows an example of the dynamic analysis process. Each of the parameters was first filtered using a five-frame running average to identify and eliminate outliers. The image quality metric (fraction of valid focal spots in the measured pupil) is used to identify partial blinks, misalignments, or data with significant corneal reflexes. Pupil size is known to correlate with accommodation response so this is also used as part of the metric. Using Eqs. (1) and (2), the MF is first computed and then the selected exam identified as the maximum value in the sequence. After the completion of a measurement, the sequence of data is analyzed, and the selected exam is displayed to the user. In Fig. 11, the vertical line indicates the location of the maximum MF as defined in Eq. (2).

Since all of the frames of data are saved during a typical acquisition, the sequence can further be played as a movie to observe fluctuations in the measurements or tear film, or individual frames of data can be extracted.

4.2 *Clinical Study*

A small clinical study was used to evaluate the effectiveness of this process. Five subjects, ages 23 to 64 were measured five times each with a 10-s sequence. Figure 12 shows variability of the measurements for both the maximum pupil (MFMPSph) and a fixed analysis pupil of 4 mm (MFAPSph). The variability was not significantly different between the two methods, although it was generally smaller for the maximum pupil method. This may be because the larger pupils generally led to more measurement samples and the smaller pupil measurements are sometimes affected by the corneal reflex. Even so, the repeatability of these methods is generally better than that of subjective methods.[30]

The measured cylinder values show even tighter reproducibility between measurements. The average variability was 0.05 D for the maximum pupil values and 0.06 D for the 4-mm analysis as shown in Fig. 13. The high-resolution WFS provides good data to give accurate astigmatism measurements. Cylinder is generally unaffected by accommodation.

For this same dataset, the range of the refraction is presented in Fig. 14. For the maximum pupil analysis, this varied on average by 0.188 and 0.33 D for the 4-mm analysis pupil. Sometimes the range was quite large, especially for the younger subjects. Most of the previous

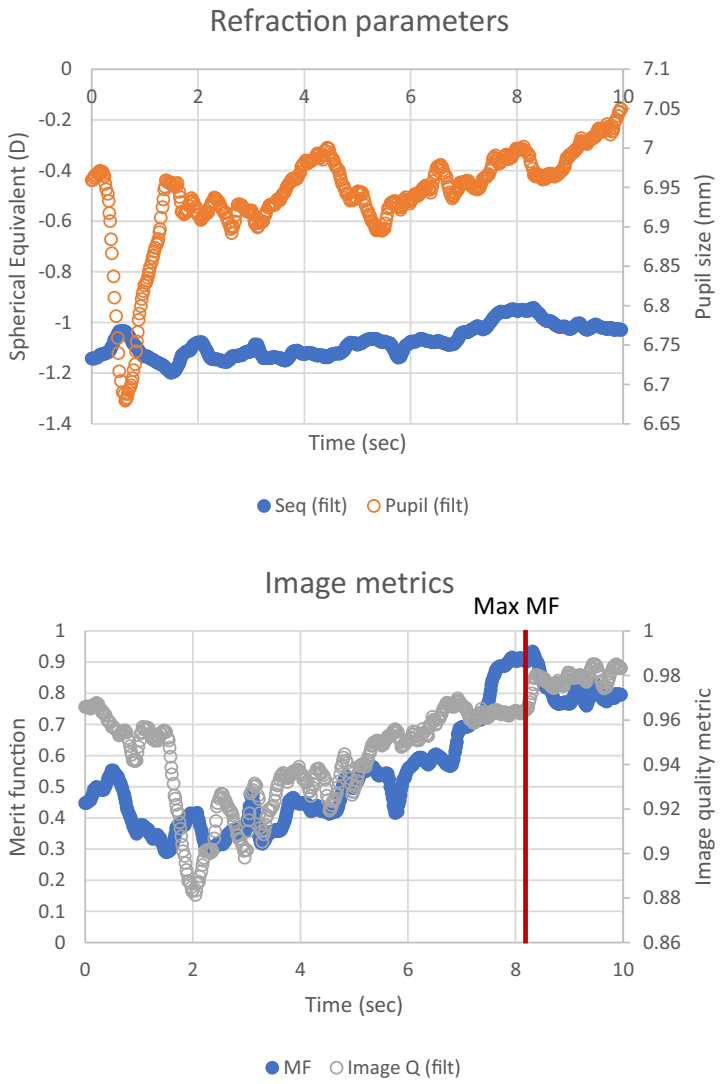

Fig. 11 (a) Refraction parameters and (b) MF. Data were first filtered to remove outliers. The vertical line indicates the location where the MF is maximized.

instruments used only a single snapshot acquired after some manual or automatic trigger. Typically, this could be 1 to 6 s after initiation of the measurement process and the timing relative to a blink is usually unknown. Thus the value recorded could be anywhere within the range presented in Fig. 14. The range of measurements during this period thus represents an inherent error in the process for single snapshot measurements. This range provides an internal estimate of the precision of any given measurement.

5 Conclusions

The combination of dynamic acquisition and analysis and a fixation target that is compensated for astigmatism have the potential for producing accurate objective measurement of refraction. The new instrument described herein has a combination of large dynamic range, wide field of view, high resolution, dynamic acquisition, and rapid analysis that makes it suitable for measurement of highly aberrated eye and associated WFG treatment.

The dynamic analysis measurement concept was evaluated and shown to be effective at reducing the range of measured sphere. Based on the limited clinical data obtained to date, the instrument repeatability is better than manifest refraction. A large-scale study would be needed

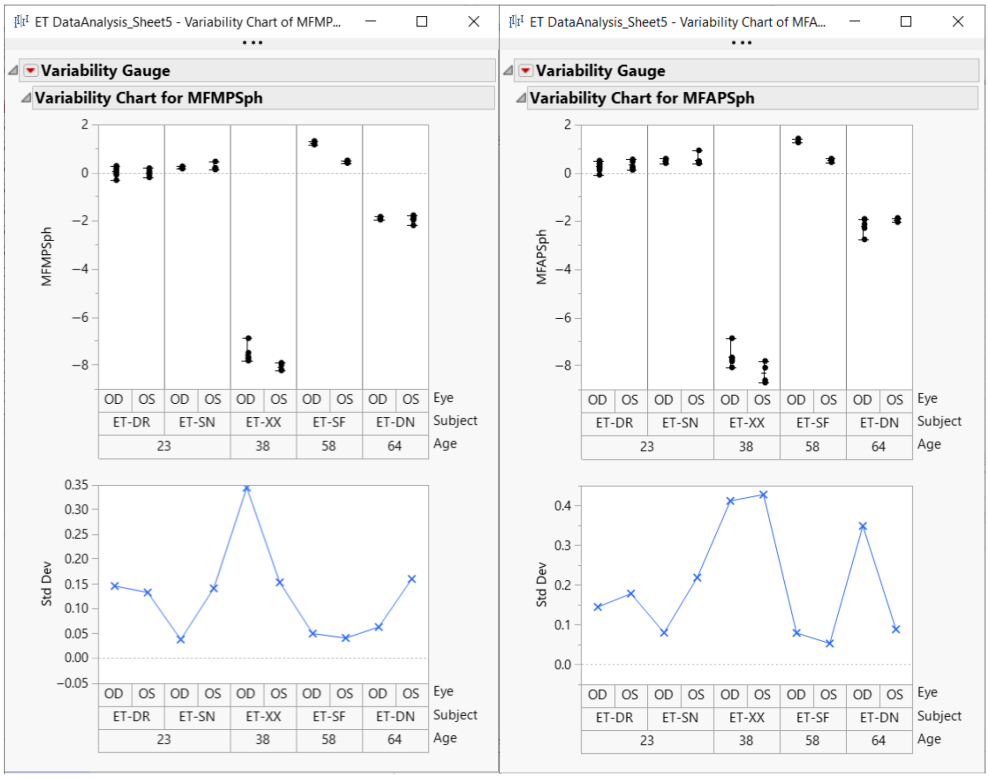

Fig. 12 Variability: mean (top) and standard deviation (bottom) of the Sphere measurements using the MF approach for (a) max pupil and for an (b) analysis pupil of 4 mm, for subjects age ranging from 23 to 64 years old.

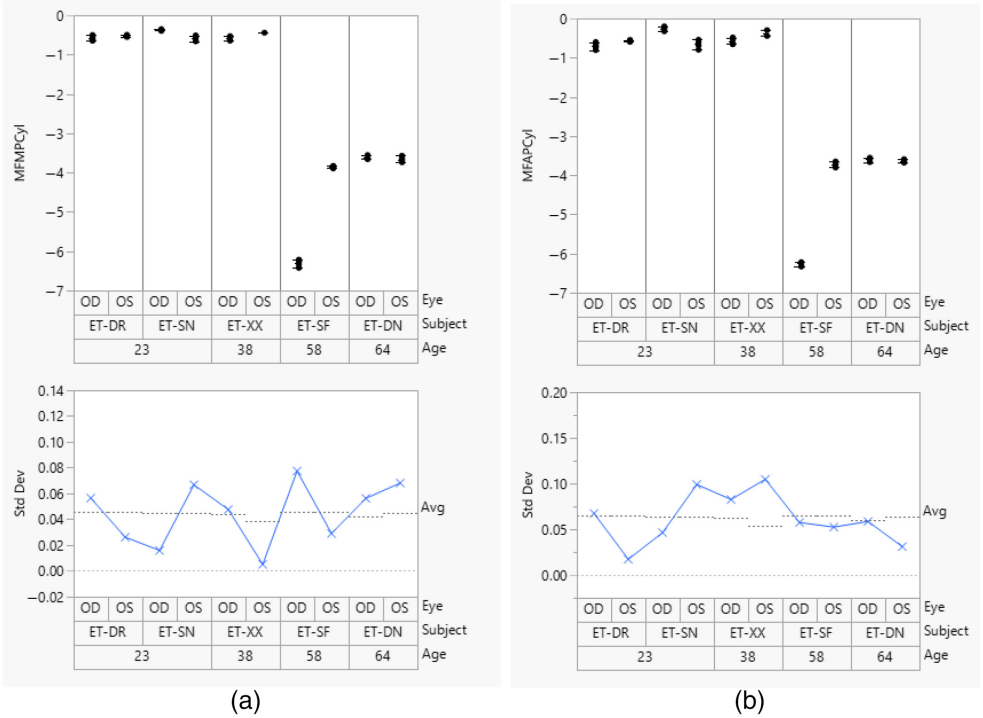

Fig. 13 Variability: mean (top) and standard deviation (bottom) of the cylinder measurements using the MF approach for (a) max pupil and for an (b) analysis pupil of 4 mm, for subjects age ranging from 23 to 64 years old.

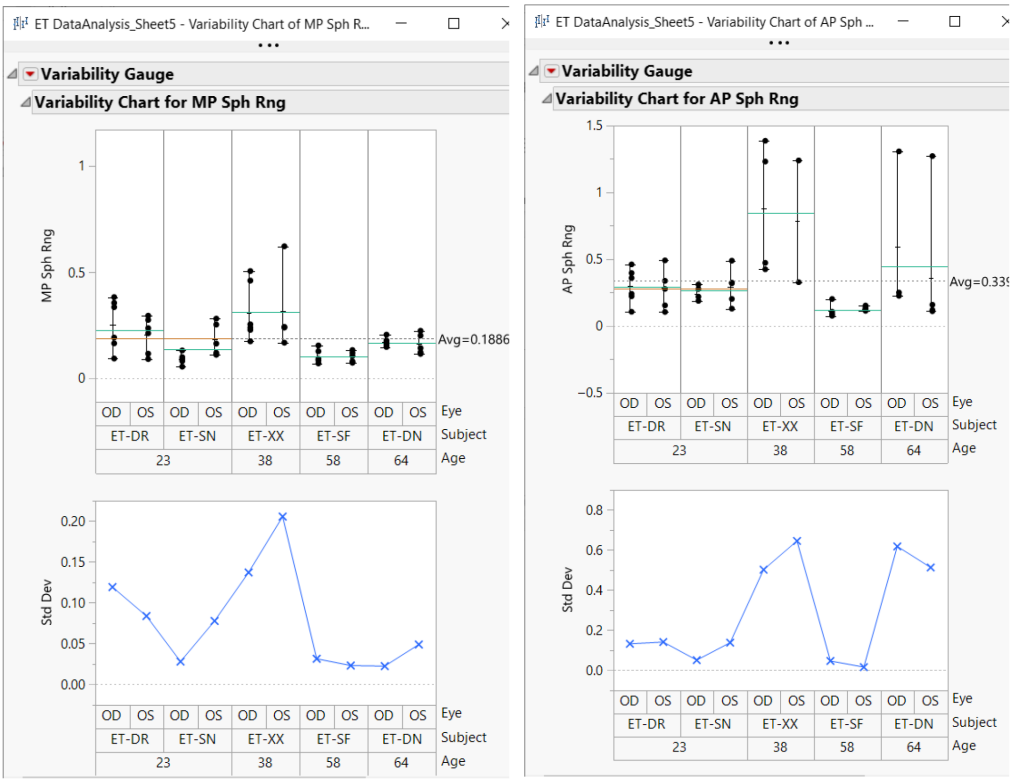

Fig. 14 Range of sphere values during the 10-s measurement sequence: (a) MP and (b) 4 mm AP.

to assess the degree of agreement between subjective and wavefront-based refraction as currently implemented in this instrument.

These results illustrate the success of improving patient care with our new instrument measurement. It presents the promise of improving performance of standard clinical tasks and hence the great potential to raise the standard of care by advancing clinical research in visual optics.

References

1. C. Scheiner, *Oculus, Sive Fundamentum Opticum*, Innspruk (1619).
2. B. R. Masters, "Ernst Abbe and his contributions to optics," in *Superresolution Optical Microscopy*, Vol. **227**, pp. 51–64, Springer (2020).
3. M. S. Smirnov, "Measurement of the wave aberration of the human eye," *Biofizika* **6**, 687–703 (1961).
4. J. Schwiegerling and D. R. Neal, "Historical development of the Shack–Hartmann wavefront sensor," in *Robert Shannon and Roland Shack: Legends in Applied Optics*, J. E. Harvey and R. B. Hooker, eds., pp. 132–139, SPIE, Bellingham, WA (2005).
5. J. Liang and D. Williams, "Aberrations and retinal image quality of the normal human eye," *J. Opt. Soc. Am. A* **14**(11), 2873–2883 (1997).
6. L. N. Thibos, "Principles of Hartmann–Shack aberrometry," *J. Refract. Surg.* **16**(5), S563–S565 (2000).
7. E. Manche and J. Roe, "Recent advances in wavefront-guided LASIK," *Curr. Opin. Ophthalmol.* **29**(4), 286–291 (2018).
8. K. Zadnik et al., "Baseline findings in the collaborative longitudinal evaluation of keratoconus (CLEK) study," *Invest. Ophthalmol. Vis. Sci.* **39**(13), 2537–2546 (1998).
9. D. Godefrooij et al., "Age-specific incidence and prevalence of keratoconus: a nationwide registration study," *Am. J. Ophthalmol.* **175**, 169–172 (2017).

10. G. D. Hastings et al., "Avoiding penetrating kerotoplasty in severe keratonconus using a wavefront-guided scleral lens," *Clin. Exp. Optometry* **105**(1), 86–88 (2022).
11. J. D. Marsack et al., "On-eye performance of custom wavefront-guided soft contact lenses in a habitual soft lens-wearing keratoconic patient," *J. Refract. Surg.* **23**(9), 960–964 (2007).
12. D. R. Neal, D. Topa, and J. R. Copland, "Effect of lenslet resolution on the accuracy of ocular wavefront measurements," *Proc. SPIE* **4245**, 14 (2001).
13. D. R. Neal, J. R. Copland, and D. Neal, "Shack–Hartmann wavefront sensor precision and accuracy," *Proc. SPIE* **4779**, 148–160 (2002).
14. R. R. Shannon et al., "Robert Shannon and Roland Shack: legends in applied optics," *Proc. SPIE*, J. Harvey et al., Ed., 628–642 (2005).
15. I. M. Bezkorovaina et al., "Qualitative assessment of the tear film in young adults," *J. Ophthalmol.* **3**, 20–25 (2019).
16. N. L. Himebaugh et al., "Use of retroillumination to visualize optical aberrations caused by tear film break-up," *Optom. Vis. Sci.* **80**(1), 69–78 (2003).
17. N. L. Himebaugh et al., "Scale and spatial distribution of aberrations associated with tear breakup," *Optom. Vis. Sci.* **89**(11), 1590–1600 (2012).
18. J. L. Nam et al., "Forward light scatter analysis of the eye in a spatially-resolved double-pass optical system," *Opt. Express* **19**(8), 7417–7438 (2011).
19. L. N. Thibos and X. Hong, "Clinical applications of the Shack–Hartmann aberrometer," *Optom. Vis. Sci.* **76**(12), 817–825 (1999).
20. C. Rosenfield, "Accommodative responses to conflicting stimuli," *J. Opt. Soc. Am. A* **8**(2), 422–427 (1991).
21. T. W. Raasch et al., "Repeatability of subjective refraction in myopic and keratoconic subjects: results of vector analysis," *Ophthalmic Physiol. Opt.* **21**(5), 376–383 (2001).
22. G. Westheimer, "Accommodation measurements in empty visual fields," *J. Opt. Soc. Am.* **47**(8), 714–718 (1957).
23. W. N. Charman and J. Tucker, "Accommodation as a function of object form," *Am. J. Optom. Physiol. Opt.* **55**(2), 84–92 (1978).
24. R. A. Applegate et al., "Importance of fixation, pupil center, and reference axis in ocular wavefront sensing, videokeratography, and retinal image quality," *J. Cataract. Refract. Surg.* **35**(1), 139–152 (2009).
25. A. Guirao and D. R. Williams, "A method to predict refractive errors from wave aberration data," *Optom. Vis. Sci.* **80**(1), 36–42 (2003).
26. L. N. Thibos et al., "Accuracy and precision of objective refraction from wavefront aberrations," *J. Vis.* **4**(9), 329–351 (2004).
27. J. Marin et al., "Unbiased estimation of refractive state of aberrated eyes," *Vis. Res.* **51**(17), 1932–1940 (2011).
28. A. Ravikumar et al., "Change in visual acuity is well correlated with change in image-quality metrics for both normal and keratoconic wavefront errors," *J. Vis.* **13**(13), 28 (2013).
29. S. Panagopoulou and D. Neal, "Zonal matrix iterative method for wavefront reconstruction from gradient measurements," *J. Refract. Surg.* **21**, S563–569 (2005).
30. M. Rosenfield and N. N. Chiu, "Repeatability of subjective and objective refraction," *Optom. Vis. Sci.* **72**(8), 577–579 (1995).

Daniel R. Neal founded WaveFront Dynamics in 2019 to continue the development of new technologies for measuring and treating eyes. At Sandia National Labs, he developed some of the first micro-optic-based wavefront sensors that he leveraged to form WaveFront Sciences Inc. WFSI further refined the technology, building instruments to measure optics, silicon wafers, and human eyes, ultimately focusing on wavefront guided LASIK. He is an OSA fellow and David Richardson Medal recipient.

Xifeng Xiao received her PhD in electrical engineering from New Mexico State University, specializing in optical engineering. She has more than 20 years of experience in wavefront technology, working on resonator analysis of high energy pulsed lasers, adaptive optics, atmospheric beam propagation, and optical simulation. At WaveFront, she is the key designer of algorithms for wavefront guided optics and vision simulation.

Richard James Copland received his BSEE degree from Oklahoma State University in 1984, his BS degree in physics/math minor degree from Oklahoma State University in 1985, and his MSEE degree from Optical Engineering University of New Mexico in 1987. He worked in remote sensing, COIL laser, fiber optics, airborne laser, and starfire optical range. He has been working with the Wavefront Sciences/Wavefront Dynamics team for 23 years. He holds over 35 patents in the fields of optical metrology and applications in optometry and ophthalmology.

Lyle Kordonowy is a lead engineer at WaveFront Dynamics. Prior to that, he was the lead mechanical engineer for Johnson and Johnson Vision and Abbot Medical Optics. He has designed optomechanical systems for ophthalmic and optometric medical devices, including the WavDyn Vision Analyzer, CatsEye cataract diagnostic device with OCT, and several metrology instruments. His prior experience was in the flight simulation industry.

Dan Hamrick gained experience in embedded real-time systems within the aerospace industry at Honeywell Flight Systems in Albuquerque. At Sandia National Laboratories, he contributed FPGA designs for image processing and radar applications. He was the lead electrical designer for embedded systems design at Wavefront Sciences. Currently, he is the lead electrical designer for the NextWave aberrometer at Wavefront Dynamics, providing motion control and dynamic vision capture through the use of embedded controllers.

Ron Rammage has 38 years of experience developing software for the defense, aerospace, laser and optics metrology, and medical industries. He has more than 20 years experience in the ophthalmic industry alone. He is an expert in SW, design control, and project management. He was the first employee and lead developer for Wavefront Sciences Inc. prior to its acquisition by AMO.

Steve Farrer has extensive experience in designing and developing optical metrology instrumentation for the medical device, aerospace, semiconductor, and telecommunication industries on projects that integrate optical, mechanical, electrical, and software components. He has worked on some high-profile projects, including James Webb Space Telescope metrology, the iDesign multifunction LASIK diagnostic instrument, and scatterometry: an optical metrology technique still used in the semiconductor industry.

Dean Rusk received his bachelor's degree in mechanical engineering from the University of New Mexico in 2021.He is a mechanical engineer at Wavefront Dynamics. In his year and a half at Wavefront Dynamics, he has assisted with the research and development of the NextWave aberrometer and various research contracts.